Three-body bound states of two bosons and one impurity in one dimension

Yanxia Liu,[1] Yi-Cong Yu,[1,2,*] and Shu Chen[1,3,4,†]

[1]*Beijing National Laboratory for Condensed Matter Physics, Institute of Physics, Chinese Academy of Sciences, Beijing 100190, China*
[2]*State Key Laboratory of Magnetic Resonance and Atomic and Molecular Physics, Wuhan Institute of Physics and Mathematics, Innovation Academy for Precision Measurement Science and Technology, Chinese Academy of Sciences, Wuhan 430071, China*
[3]*School of Physical Sciences, University of Chinese Academy of Sciences, Beijing 100049, China*
[4]*Yangtze River Delta Physics Research Center, Liyang, Jiangsu 213300, China*

(Received 29 April 2021; accepted 23 August 2021; published 2 September 2021)

We investigate one-dimensional three-body systems composed of two identical bosons and one mass-imbalanced atom (impurity) with attractive two-body and three-body zero-range interactions. In the absence of three-body interaction, we give a complete phase diagram of the number of three-body bound states in the whole region of mass ratio and the ratio of intra- and intercomponent interaction strength via direct calculation of Skornyakov-Ter-Martirosyan equations. We demonstrate that other low-lying three-body bound states emerge when the mass of the impurity particle is different from other two identical particles. We obtain the binding energies together with the corresponding wave functions. When the mass of impurity atom is very large, there are at most three three-body bound states. In the presence of three-body zero-range interaction, we reveal that weak three-body interaction will not always induce one more three-body bound state. At some special parameter points, arbitrary small three-body interaction can generate one more three-body bound state. This corresponds to the transition of the number of three-body bound states induced only by two-body attractive interaction.

DOI: 10.1103/PhysRevA.104.033303

I. INTRODUCTION

The quantum three-body problem has drawn numerous concerns and is of central interest in the study of few-body physics [1–4]. In the past decades, continuous efforts have led to many theoretical breakthroughs [5–8], including the derivation of the well-known Skornyakov-Ter-Martirosyan (STM) equations which can be used to calculate the wave functions and spectra of quantum identical three-body system with short-range interactions [5], Faddeev's formulism of the three-body problem with discrete and continuum spectra [6], and the finding of a distinctive Efimov effect in the spectrum and trimer states of the three-boson system [7,8]. The three-boson system with short-range interactions can exhibit an infinite number of trimer states fulfilling a discrete symmetry, which is called the Efimov effect. The first experimental evidence of the Efimov effect came from ultracold gases [9]; this early evidence stimulated intensive studies of few-body ultracold physics in different dimensions [4,10–20]. Experiments with a few cold atoms provide unprecedented control of both the atom number with unit precision and the interatomic interaction strength by the combination of sweeping a magnetic offset field and the confinement-induced resonance [21].

Recently, three-body systems in one dimension have gained a great deal of attention [20,22–30]. As the basis of quantum integrability, the Yang-Baxter equation describes the two-body scattering matrix fulfilling a certain intertwined relation with at least three particles, and thus three-body systems become important candidates for studying the integrability and its breakdown [31–35]. An integrable three-boson system with two-body attractive interactions is known to have only a three-body bound state [36,37]. In general, the introduction of mass imbalance and three-body interaction will break the integrability condition. Nevertheless, it has been shown that the imbalanced three-body systems exhibit more rich physics than the integrable systems which are composed of three identical atoms [25–28]. The zero-range three-body forces in a quasi-one-dimensional system can be induced by the virtual excitations of pairs of atoms in the waveguide [31,32,38,39], which may realize the quantum droplets in a one-dimensional (1D) system [40–42]. For 1D interaction systems, some physical properties will not disappear in the presence of three-body interaction, for example, Bose-Fermi mapping [43–48]. For the system of three identical particles with attractive three-body interaction, there exists an excited trimer state in the vicinity of the dimer threshold [22,23].

Most of the theoretical studies on mass-imbalanced systems in one dimension have focused on the heavy-heavy-light (HHL) system [25–28], in which case the Born-Oppenheimer approximation (BOA) and the adiabatic hyperspherical approximation work relatively well. This system has a rich three-body bound-state spectrum and the number of bound states increases with increasing heavy-light mass ratio. Meanwhile, the experimental realizations of mass-imbalanced systems have made tremendous progress, such as fermionic mixtures [49–52] and bosonic-fermionic mixtures [53–58], which has stimulated us to investigate theoretically

*ycyu@wipm.ac.cn
†schen@iphy.ac.cn

mass-imbalanced three-body systems in the whole parameter region and beyond the BOA.

In this work we study 1D three-body systems composed of two identical bosons and one impurity with zero-range two-body and three-body interactions by solving the momentum-space STM equations. We first study the case in the absence of three-body interaction and present the phase diagram of the number of bound states in the parameter space spanned by the mass ratio and the ratio of the intra- and intercomponent interaction strengths. We find significant differences between light-light-heavy (LLH) and HHL systems. In particular, we reveal that the LLH system possesses at most three three-body bound states with attractive interactions. We then study the effect of three-body zero-range interaction and derive the corresponding STM equations. At some special parameter points, one more three-body bound state induced by three-body interaction for arbitrary strength appears, to be compared with the cases with only two-body attractive interaction. These points correspond to the transition points of the number of three-body bound states induced only by two-body attractive interaction.

Our article is organized as follows. In Sec. II we introduce our model and in Sec. III we describe the method for solving our three-body problem in detail. In particular, we develop some computational techniques to calculate the STM equation by mapping it to the solution of linear equations, which enables us to get the complete phase diagram of the number of three-body bound states in the whole parameter region, which is shown in Sec. IV. We also present the exact Bethe-ansatz solution of the odd-parity bound state in the limit case where the impurity is infinitely heavy. In Sec. V the three-body interaction is introduced and we show how the mass ratio and the ratio of coupling strengths effect the forming of a three-body bound state induced by the three-body interaction. A summary is given in Sec. VI.

II. MODEL

The general Hamiltonian for a three-particle system composed of two identical bosons (1 and 2) with mass M and an impurity particle (3) with mass m in one dimension [25] is given by

$$\hat{H} = -\frac{\hbar^2}{2M}\left(\frac{\partial^2}{\partial x_1^2}+\frac{\partial^2}{\partial x_2^2}\right) - \frac{\hbar^2}{2m}\frac{\partial^2}{\partial x_3^2} + d_0\delta(x_1-x_2) + g_0\delta(x_1-x_3) + g_0\delta(x_2-x_3), \tag{1}$$

where the attractive boson-boson (BB) and boson-impurity (BI) interactions are described by zero-range δ functions with coupling constants $d_0 < 0$ and $g_0 < 0$. Note that the total momentum $\hat{P} = \sum_i -i\hbar\frac{\partial}{\partial x_i}$ is conserved. Thus, by introducing the Jacobi coordinates

$$x = x_3 - \frac{x_1+x_2}{2}, \quad y = \frac{\sqrt{2M/m+1}}{2}(x_1-x_2), \tag{2}$$

the time-independent Schrödinger equation of (1) with its binding energy $E = -\hbar^2\kappa^2/2\mu_{12,3}$ can be reduced in the center-of-mass frame as

$$\left[-\left(\frac{\partial^2}{\partial x^2}+\frac{\partial^2}{\partial y^2}\right) + g\delta(x\sin\theta - y\cos\theta) + g\delta(x\sin\theta + y\cos\theta) + d\delta(y) + \kappa^2\right]\psi = 0, \tag{3}$$

where $\mu_{12,3} = 2Mm/(2M+m)$, $\theta = \arctan\sqrt{1+2M/m}$, and the rescaling coupling constants are

$$d = d_0\frac{\mu_{12,3}}{\hbar^2}\sqrt{1+2M/m} = -\frac{4}{\tan\theta a_{\mathrm{BB}}},$$
$$g = g_0\frac{2\mu_{12,3}}{\hbar^2}\sqrt{\frac{1+2M/m}{2+2M/m}} = -\frac{2\sqrt{2+2M/m}}{\tan\theta a_{\mathrm{BI}}}. \tag{4}$$

The BB and BI scattering lengthes are $a_{\mathrm{BB}} = -\hbar^2/\mu_{\mathrm{BB}}d_0$ and $a_{\mathrm{BI}} = -\hbar^2/\mu_{\mathrm{BI}}g_0$, with $\mu_{\mathrm{BB}} = M/2$ and $\mu_{\mathrm{BI}} = Mm/(M+m)$, respectively. The limitations $M/m \to \infty$ and $M/m \to 0$ are represented by $\theta \to \pi/2$ and $\theta \to \pi/4$, respectively. In addition, $\theta = \pi/3$ corresponds to the equal-mass case.

III. METHOD: STM EQUATIONS

The Hamiltonian (1) was investigated in several articles [25,28] with $M/m > 1$ and has been of great interest in recent experiments [59]. It has been confirmed that in the limits $|g_0/d_0| \to 0$ and $|g_0/d_0| \to \infty$ there exists a critical value of the mass ratio M/m where three-body bound states emerge and the $(2+1)$-scattering length vanishes. However, previous studies relied on the BOA in the strong-coupling (weak-coupling) limit on the premise of $M/m \gg 1$ [60]. The BOA is not proper near $M/m = 1$ or $M/m < 1$ and will lead to the loss of important information on the bound states.

In this work we adopt the method developed in [22,23] to transform the Hamiltonian (3) into three coupled integral equations. Solving these integral equations provides the wave functions of bound states and eigenenergies and further gives the full phase diagram of the number of bound states. The time-independent Schrödinger equation (3) in momentum space reads

$$(p_x^2+p_y^2+\kappa^2)u(p_x,p_y) + \sum_{i=1}^{3}\frac{g_i}{2\pi}\int dl_i^{\perp}u(k_x,k_y) = 0, \tag{5}$$

where $g_1 = d$, $g_2 = g_3 = g$, E is the eigenenergy, and $u(p_x,p_y)$ is the wave function in momentum space $u(p_x,p_y) = \int\frac{dx\,dy}{2\pi}\psi(x,y)e^{i(-p_xx-p_yy)}$. The $dl_i^{\perp}$ denotes the line integral of the complex scalar field $u(k_x,k_y)$ with the path parametrized by $k_x = d_i\cos\theta_i - t_i\sin\theta_i$ and $k_y = d_i\sin\theta_i + t_i\cos\theta_i$, where $t_i = -k_x\sin\theta_i + k_y\cos\theta_i$ is the arclength parameter and $d_i = p_x\cos\theta_i + p_y\sin\theta_i$, representing the integral line $l_i^{\perp}$ that goes through the point (p_x,p_y) and being vertical to line l_i (see Fig. 1). Here $\theta_1 = 0$, $\theta_2 = \theta$, $\theta_3 = -\theta$, and θ solely depends on the mass ratio M/m [see Eq. (4)]. Note that after integrating along line $l_i^{\perp}$, the results can be arranged as a one-parameter function $f_i(d_i) = \int dl_i^{\perp}u(k_x,k_y)$

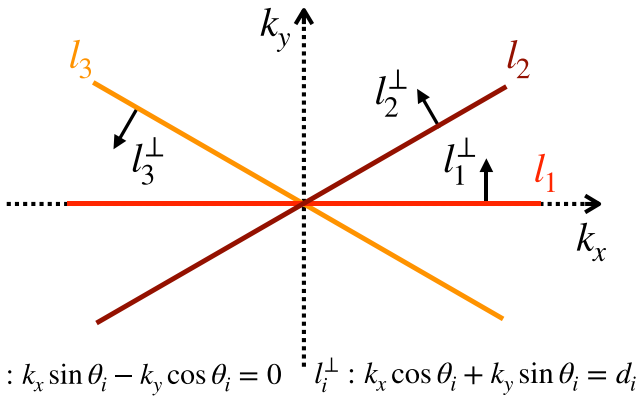

FIG. 1. Schematic of the Hamiltonian (3). The solid lines represent the δ potentials.

and the Schrödinger equation (5) becomes

$$\left(p_x^2 + p_y^2 + \kappa^2\right)u(p_x, p_y) + \sum_{i=1}^{3} \frac{g_i}{2\pi} f_i(d_i) = 0. \tag{6}$$

The integration of Eq. (6) over $l_i^\perp$ leads to

$$\left(1 + \frac{g_i}{2\sqrt{k^2+\kappa^2}}\right) f_i(k) = \sum_{j\neq i} \int \frac{dk'}{2\pi} \frac{-g_j |\sin(\theta_i - \theta_j)| f_j(k')}{k'^2 + k^2 - 2kk'\cos(\theta_i - \theta_j) + \kappa^2 \sin^2(\theta_i - \theta_j)} \tag{7}$$

for $i = 1, 2, 3$, which are the STM equations in momentum space. Substituting $f_i(k)$ into (6) and then taking the Fourier transformation, the solutions of the Schrödinger equation (3) are obtained.

Two remarks are necessary for solving (7): First, the self-consistent condition $\int dk_x dk_y u(k_x, k_y) = \int dk f_i(k)$ can be proved by integrating (7) by both sides; second, the Hamiltonian (3) obviously possesses exchange symmetry of two bosons and parity symmetry, which are reflected in the eigenstates of (3) by $\psi(x, y) = \psi(x, -y)$ and $\psi(x, y) = \pm\psi(-x, -y)$, and these two discrete symmetries are well represented in (7) by $f_2(k) = f_3(k)$ for $\psi(x, y) = \psi(x, -y)$ and $f_i(k) = \pm f_i(-k)$ $(i = 1, 2, 3)$ for $\psi(x, y) = \pm\psi(-x, -y)$, respectively. The solutions $f_i(k)$ of STM equations (7) have no pole in the bound-state sector; thus $f_i(k)$ can be safely discretized numerically. The analysis of the scattering sector by (7) is much more sophisticated because the singularities of the wave function $u(p_x, p_y)$ need careful handling. In this work we concentrate on the bound-state sector only.

After discretization, the STM equation (7) becomes a set of linear equations and the nonzero solutions satisfying $E < E_{\text{th}}$ are the bound states. Here $E_{\text{th}} = -\hbar^2 \max[(g_i/2)^2]/2\mu_{12,3}$ defines the two-body threshold energy and serves as the lower bound of the continuous spectra. Specifically, consider the combination of the three functions $f_1(k)$, $f_2(k)$, and $f_3(k)$ as a vector $[f_1(k), f_2(k), f_3(k)] \to \boldsymbol{V}$; then the three STM equations (7) become a matrix equation $\boldsymbol{M}(E)\boldsymbol{V} = \boldsymbol{V}$. The existence of a nonzero solution of equation $\det[\boldsymbol{M}(E) - I] = 0$ gives the spectrum of the Hamiltonian.

For given g_i and θ_i, to obtain the nonzero solution $f_i(k)$ in (7), we need to search for the discrete energies $-\kappa^2$, which is a difficult task. However, we can bypass this difficulty by solving the eigenvalue problem

$$\left(-\lambda + \frac{g_i}{2\sqrt{x^2+\tilde{\kappa}^2}}\right)\tilde{f}_i(x) = \sum_{j\neq i} \int \frac{dy}{2\pi} \frac{-g_j |\sin(\theta_i - \theta_j)| \tilde{f}_j(y)}{y^2 + x^2 - 2xy\cos(\theta_i - \theta_j) + \tilde{\kappa}^2 \sin^2(\theta_i - \theta_j)}, \tag{8}$$

where λ, which can be numerically proved to be negative definite, on the left-hand side is the eigenvalue and $\tilde{\kappa}$ is set to be a unit whose value can be arbitrarily chosen (for convenience, we set $\tilde{\kappa} = 1$). In this sense, solving λ gives us the solution of Eq. (7) as $\kappa = \lambda\tilde{\kappa}$. The functions $f_j(k)$ can be obtained by taking $f_j(k) = \tilde{f}_j(k/\lambda)$. Moreover, we find that the number of bound states only depends on the mass ratio M/m and the coupling strength ratio d/g (or d_0/g_0). This phenomenon is comprehensible due to the scaling property of the Hamiltonian (3). Note that after the scaling transitions $x' \to \lambda x$ and $y' \to \lambda y$, the coupling constants d and g are rescaled as $g' \to g/\lambda$ and $d' \to d/\lambda$ while the spectrum is rescaled as $\epsilon_n' \to \lambda^{-2}\epsilon_n$. This scaling property keeps the structure of the spectra invariant; thus the number of bound states remains constant for fixed M/m and d/g. However, when the three-body interaction is presented, this scaling property is broken. This will be discussed in Sec. V.

IV. PHASE DIAGRAM AND EMERGED THREE-BODY BOUND STATES

Although the limit cases $M/m \to \infty$ and $|d|/|g| \to 0$ or ∞ have been discussed by Kartavtsev *et al.* [25] and Mehta [26] under the one-channel approximation and BOA, there are many regions of M/m and d/g that still remain unexplored. By exactly solving the integral equation (7), we get the wave function and present the full phase diagram of the number of bound states in the parameter space spanned by $\sqrt{M/m}$ and $|d|/|g|$ (see Fig. 2). In the region $M/m > 1$, the number of bound states is in agreement with the results in Refs. [26,27]. The phase diagram provides rich information near the integrable point $(|d|/|g| = 1, M/m = 1)$. This shows that in the equal-mass case there is always only one bound state. Near the integrable point the phase diagram is sensitive to M/m: When $|d|/|g| = 1$, one more three-body bound state will emerge even though M/m is slightly changed. When $M/m = 1$, the number of three-body bound states remains constant with varying $|d|/|g|$.

Moreover, in the HLL region $M/m < 1$, Fig. 2 shows the emergence of extra excited three-body bound states near $g = d$. For clarity, we present the binding energies of three-body bound states as a function of d with $M/m = 0.01$ and $g = -1$ in Fig. 3(a). It is found that three three-body bound states exist when $d/g \to 1$, one with odd-parity symmetry (the middle one) and two with even-parity symmetry.

In the limit $M/m \to 0$ (or $\theta \to \pi/4$) with arbitrary parameters g and d, there exists a Bethe-ansatz solution for the

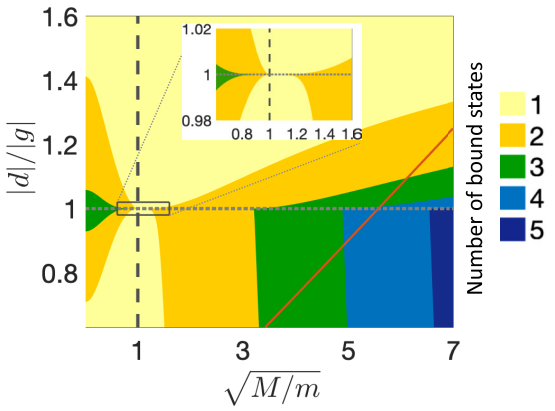

FIG. 2. Phase diagram of the number of three-body bound states. The X axis is the square root of the mass ratio and the Y axis is the ratio of the absolute value of the coupling strength d and g. Here we consider the attractions with $d < 0$ and $g < 0$. The red (dark gray) solid line represents the relation between $|d|/|g|$ and $\sqrt{M/m}$ with $|g_0|/|d_0| = 4$, where $|d|/|g| = |d_0|/|g_0|\sqrt{1/2(1 + M/m)}$.

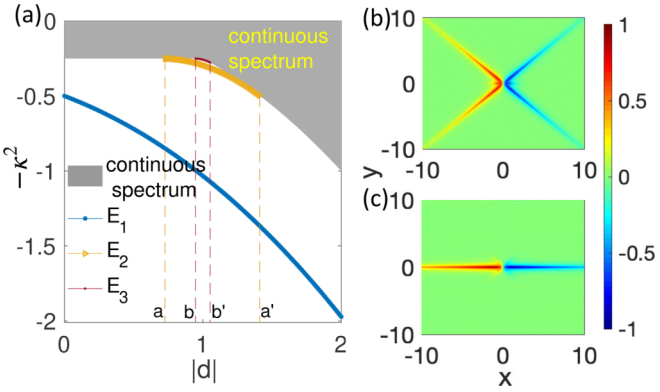

FIG. 3. (a) Binding energies of three-body bound states as a function of d with $M/m = 0.01$ and $g = -1$. The gray area denotes the continuous spectrum. The orange (light gray) dashed lines denote the critical values where the odd-parity excited three-body bound state emerges at $|d| = a = 0.707$ and disappears at $|d| = a' = 1.414$ The red (dark gray) dashed lines denote the critical values where the even-parity excited three-body bound state emerges at $|d| = b = 0.929$ and disappears at $|d| = b' = 1.058$. The wave functions of the odd-parity excitation states [the yellow line with triangle markers in (a)] are shown near the critical values (b) $|d| \to a$ and (c) $|d| \to a'$.

odd-parity wave function of the Hamiltonian (3) with energy $E = -\hbar^2(\kappa_1^2 + \kappa_2^2)/2\mu_{12,3}$,

$$\psi(x, y) = \begin{cases} C\left(\frac{d-\sqrt{2}g}{d-g/\sqrt{2}}e^{-\kappa_1 x-\kappa_2 y} + \frac{g}{\sqrt{2}d-g}e^{-\kappa_2 x-\kappa_1 y} - e^{-\kappa_2 x+\kappa_1 y}\right) & \text{for } 0 < y < x \\ C(e^{-\kappa_1 x-\kappa_2 y} - e^{\kappa_1 x-\kappa_2 y}) & \text{for } y > |x|, \end{cases} \tag{9}$$

where $\kappa_1 = d/2 - g/\sqrt{2}$, $\kappa_2 = -d/2$, and C is the normalization factor of the wave function. The wave function in other regions can be obtained through the symmetries of the wave function: $\psi(x, y) = \psi(x, -y)$ and $\psi(x, y) = -\psi(-x, -y)$. The wave function in Eq. (9) is confined in $y = 0$ or $x = \pm y$, which is not necessarily bounded in those directions. The existence of this bounded state puts constraint conditions on g and d. Along $y = 0$, the wave function vanishes at $|x| \to \infty$, which gives us $\kappa_1 > 0$ and $\kappa_2 > 0$, and thus $d > \sqrt{2}g$. Along $x \pm y = 0$, the wave function vanishes at $|x \mp y| \to \infty$, which gives us $\kappa_2 - \kappa_1 > 0$ and $\kappa_1 + \kappa_2 > 0$, and thus $g/\sqrt{2} > d$. Taken together, the odd-parity bound state exists within $g/\sqrt{2} > d > \sqrt{2}g$. The even-parity bound states cannot be solved via the Bethe ansatz. We show the energies of the bound states with $M/m = 0.01$ in Fig. 3(a). The even-parity bounded state (marked by the red line with point markers) emerges from the continuous spectrum from $|d| = 0.929$ to $|d| = 1.058$. The numerical computation of the odd-parity bound state (marked by the yellow line with triangle markers) emerges from $|d| = 0.707 \approx 1/\sqrt{2}$ to $|d| = 1.414 \approx \sqrt{2}$, which is in agreement with the analytical result obtained before. Figure 3(b) confirms that near $|d| = 0.707$ one light particle is combined tightly with the heavy one, forming a molecule, which is loosely combined with the other light particle. Figure 3(c) shows that the two light particles form a dimer, which is loosely combined with the heavy one at $|d| = 1.414$. Figures 3(b) and 3(c) also reveal something about the threshold of atom-dimer continuous spectra. When $|d| < 1$ and $|d| < |g|$, the trimer state exhibits, near threshold, one heavy particle and one light particle bound tightly, as shown in Fig. 3(b), which suggests that the dimer at the bottom of the threshold is formed by a heavy particle and a light particle. When $|d| > 1$ and $|d| > |g|$, the dimer at the bottom of the threshold consists of two light particles, which can be inferred from Fig. 3(c) with similar reasoning.

V. EFFECTS OF THREE-BODY INTERACTION

It was discussed in Sec. III that the scaling property of the Schrödinger equation (3) results in the structure of the spectra relying only on M/m and d/g. However, the three-body attraction breaks this scaling property and may cause significant consequences [22,23,40,61]. The three-body zero-range interaction can be introduced by adding the term $\hat{H}^{(3)} = t_0\delta(x_3 - x_1/2 - x_2/2)\delta(x_1 - x_2)$ in (1), which corresponds to adding the term

$$\hat{H}^{(3)}_{\text{red}} = t_B\delta(x)\delta(y) \tag{10}$$

to the Schrödinger equation (3), where $t_B = \frac{2t_0}{\sqrt{2M/m+1}}$. Similar to (5), the Schrödinger equation in momentum space is given by

$$-\left(p_x^2 + p_y^2 + \kappa^2\right)\frac{u(p_x, p_y)}{c_3} - \sum_{i=1}^{3}\frac{g_i}{2\pi}\frac{f_i(d_i)}{c_3} = 1, \tag{11}$$

where g_i, d_i, and f_i are the same as defined in Sec. III and

$$c_3 = \frac{t_B}{4\pi^2}\int_{-\infty}^{\infty} dk_x dk_y u(k_x, k_y) \tag{12}$$

represents the three-body interaction in momentum space. However, the wave function $u(k_x, k_y)$ in momentum space is proportional to $-c_3/(p_x^2 + p_y^2 + \kappa^2)$. Equation (12) experiences logarithmic divergence when integrating in the whole momentum space, which suggests the requirement of a renormalization procedure for the three-body interaction strength t_B.

Based on the Schrödinger equation (11) and the same method developed in Sec. III, the STM equation with three-body interaction is obtained by adding an extra term $-c_3\pi/\sqrt{k^2+\kappa^2}$ into (7), which gives

$$\left(1+\frac{g_i}{2\sqrt{k^2+\kappa^2}}\right)F_i(k) = -\frac{\pi}{\sqrt{k^2+\kappa^2}} + \sum_{j\neq i}\int \frac{dk'}{2\pi}\frac{-g_j|\sin(\theta_i-\theta_j)|F_j(k')}{k'^2+k^2-2kk'\cos(\theta_i-\theta_j)+\kappa^2\sin^2(\theta_i-\theta_j)}, \tag{13}$$

where $F_i(k) = f_i(k)/c_3$. For fixed g_i and M/m, with any real c_3, Eq. (13) gives a unique $F_i(k)$. In solving $F_i(k)$, we encounter the matrix $\boldsymbol{M}(E) - \boldsymbol{I}$, which is invertible in the bound-state sector except for the isolate points [62], which correspond to the discrete bound energies in (7).

The solutions of Eqs. (7) and (13) are different in ultraviolet behaviors. It can be proved that $f_i(k) \propto 1/k^2$ in (7) and $F_i(k) \approx -\pi/\sqrt{k^2+\kappa^2}$ in (13), whose derivations are given in the Appendix. Since a function which decays faster with large momentum is preferable in numerical methods, it is convenient to introduce the substitution of $F_i(k) = -\pi/\sqrt{k^2+\kappa^2} + h_i(k)$ for $F_i(k)$, where $h_i(k) \propto 1/k^2$ at $k \to \infty$. Putting this relation into (13), the integral equation for $h_i(k)$ is obtained as

$$\left(1+\frac{g_i}{2\sqrt{k^2+\kappa^2}}\right)h_i(k) = -\pi\sum_j g_j\eta(k,\kappa^2,|\theta_i-\theta_j|) + \sum_{j\neq i}\int \frac{dk'}{2\pi}\frac{-g_j|\sin(\theta_i-\theta_j)|h_j(k')}{k'^2+k^2-2kk'\cos(\theta_i-\theta_j)+\kappa^2\sin^2(\theta_i-\theta_j)}, \tag{14}$$

with the analytic function $\eta(k,\kappa^2,\theta)$ defined by

$$\eta(k,\kappa^2,\theta) = \frac{-\frac{1}{2\pi}|\sin\theta|}{\sqrt{k^2+\kappa^2}(k^2+\kappa^2\cos^2\theta)} \times\left(2|k|\operatorname{arcoth}\frac{\sqrt{k^2+\kappa^2}}{|k|} + \frac{(\pi-2\theta)\sqrt{k^2+\kappa^2}}{\tan\theta}\right)$$

and $\eta(k,E,0) \triangleq \lim_{\theta\to 0}\eta(k,E,\theta) = -(2k^2+2\kappa^2)^{-1}$.

Substituting Eq. (11) into (12), we can get

$$\frac{1}{t_B} = -\frac{1}{4\pi}\ln\frac{\Lambda^2+\kappa^2}{\kappa^2} - \frac{1}{4\pi^2}\sum_i\int_\Lambda \frac{dS}{2\pi}\frac{g_iF_i(d_i(p_x,p_y))}{p_x^2+p_y^2+\kappa^2}, \tag{15}$$

where $\int_\Lambda dS \triangleq \int_{p_x^2+p_y^2<\Lambda^2} dp_x dp_y$ is the two-dimensional integral with cutoff $\Lambda > 0$. We apply the momentum-cutoff regularization scheme [63,64] with momentum cutoff Λ.

The relation between the bare coupling constant t_B and the renormalized coupling constant t_R can be written as

$$\frac{1}{t_B} = \frac{1}{t_R} - \frac{1}{4\pi}\ln\frac{\Lambda^2}{\mu^2}, \tag{16}$$

where μ^2 is the emerged energy scale. The renormalized coupling constant t_R is obtained by cutting off the logarithmically divergent part in t_B with scaling μ [65,66].

Substituting Eq. (16) into (15) and replacing $F_i(k)$ with $-\pi/\sqrt{k^2+\kappa^2} + h_i(k)$ in Eq. (15), we arrive at the relation between the solution $h_i(k)$, the renormalized coupling constant t_R, and the energy scale μ^2:

$$\frac{1}{t_R} = \frac{1}{4\pi}\ln\frac{\kappa^2}{\mu^2} + \sum_i\frac{g_i}{8}\left(\frac{1}{\kappa} - \frac{1}{\pi^2}\int dk\frac{h_i(k)}{\sqrt{k^2+\kappa^2}}\right). \tag{17}$$

Equations (14) and (17) completely determine the relation between g_i, θ_i, μ, t_R, and κ^2. We begin with one parameter t_B; the renormalization scheme introduces two quantities t_R and μ for the three-body interaction. The physical three-body coupling strength the particles experience is t_R. However, since we can choose t_R arbitrarily, the renormalized three-body interaction can be described by one scaled parameter only [64,67]. To this end we introduce the three-body scattering length a_3, which describes the asymptotic behavior of the wave function $\Psi = \psi/c_3 \propto \ln\frac{\rho}{a_3}$ when $\rho = \sqrt{x^2+y^2} \to 0$ [22]. To obtain a_3 we need to expand the wave function at $\rho \to 0$,

$$\Psi(\rho) = -K_0(|\kappa\rho|) + 2\pi\left(\frac{1}{t_R} - \frac{1}{4\pi}\ln\frac{\kappa^2}{\mu^2}\right), \tag{18}$$

which can be obtained by solving $u(p_x,p_y)/c_3$ from (11) and transforming it to coordinate space, where $K_0(x)$ is the modified Bessel function of the second kind and has the asymptotic behavior $K_0(|x|) \approx -\ln|\frac{x}{2}| - \gamma$ at $|x| \to 0$ with Euler constant $\gamma \approx 0.577\,22$. Substituting it into (18), we arrive at the close form of a_3,

$$-\ln\frac{a_3}{2} = \gamma + \frac{2\pi}{t_R} + \ln\mu, \tag{19}$$

where $a_3 > 0$ for the right-hand side of (18) is real. Equations (14), (17), and (19) give the relation between two-body scattering lengths and three-body scattering lengths. In solving Eqs. (14), (17), and (18), the same difficulty arises as in Eq. (7): It is not easy to solve κ^2 for a given a_3. The opposite is undemanding, and we handle this difficulty in the same manner as in Sec. III, i.e., we search for the three-body scattering length a_3 for given κ^2 and two-body coupling constants d and g.

We have discussed in Sec. IV that the system with only two-body interactions can exhibit multiple three-body bound states. It has been proved that the three-body interaction alone can exhibit one three-body bound state with energy $E = -\hbar^2\kappa^2/2\mu_{12,3} = -4\hbar^2e^{-2\gamma}/2a_3^2\mu_{12,3}$ [40,64]. References [22,23] showed that when $M = m$ and $d_0 = g_0 < 0$,

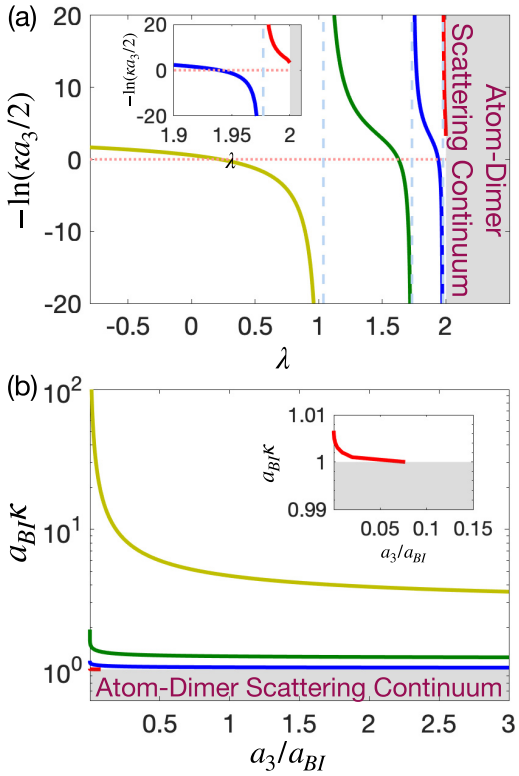

FIG. 4. Binding energies for the system with $M/m = 16$ and $g_0/d_0 = 4$ in the presence of three-body interaction. (a) Relation between $-\ln\frac{\kappa a_3}{2}$ and λ, where a_3 is the three-body scattering length and $\lambda = -g/\kappa$ (κ is regarded as the unit for two-body and three-body scattering lengths). The two-body coupling constant d is then expressed as $d = -\lambda\kappa\frac{d_0}{g_0}\sqrt{\frac{m+M}{2m}}$ [refer to the relation (4)]. The threshold $E_{\rm th} = -\hbar^2(g/2)^2/2\mu_{12,3}$ also corresponds to $\lambda = 2$ ($\kappa = -g/2$). (b) Binding energy related parameter $a_{\rm BI}\kappa$ (the binding energy $E = -\hbar^2\kappa^2/2\mu_{12,3}$) as a function of the three-body to two-body BI scattering length ratio $a_3/a_{\rm BI}$. The gray area represents the atom-dimer scattering continuum.

one more three-body bound state would emerge once the three-body interaction is introduced. Now an interesting question arises: For the mass-imbalanced system with attractive two-body interaction, does the system exhibit additional three-body bound states with arbitrarily tuned three-body interaction? The answer is negative. In certain parameter regions, there is no additional three-body bound state, as one can see from Fig. 4. In Fig. 4 we demonstrate three-body bound states with $M/m = 16$ and $g_0/d_0 = 4$. For given $\lambda = -g/\kappa$, the three-body scattering length is determined uniquely. As λ increases, $-\ln\frac{\kappa a_3}{2}$ repeatedly runs from $+\infty$ to $-\infty$ monotonically and continuously, which is shown in Fig. 4(a). Figure 4(b) can be obtained from a coordinate transformation of Fig. 4(a). When $a_3/a_{\rm BI} \to \infty$ ($t_R = 0$), there remain three three-body bound states, which are induced only by two-body interaction. For arbitrary three-body interaction, those three states always exist. For $a_3/a_{\rm BI} < 0.076$, an additional three-body bound state emerges out of the atom-dimer continuum, which is induced by three-body interaction. This puts an upper bound on $a_3/a_{\rm BI}$ as $a_{\rm max,BI} = 0.076$, below which there exists the additional three-body bound state.

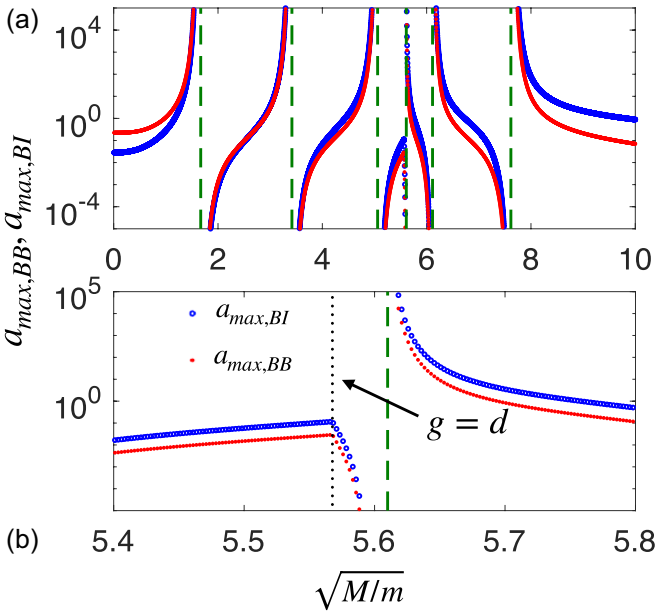

FIG. 5. (a) Maximum three-body scattering length in units of the two-body BB (BI) scattering length $a_{\rm BB}$ ($a_{\rm BI}$) vs the square root of the mass ratio $\sqrt{M/m}$ at the two-body threshold for the system with the two-body coupling $g_0/d_0 = 4$. The dotted line is $\sqrt{M/m} = 5.57$, which corresponds to $g = d$. (b) Close-up of the area near $\sqrt{M/m} = 5.57$.

From the analysis above, we conclude that the three-body interaction cannot always introduce one more three-body bound state, which depends on the mass ratio and the three-body and two-body scattering lengths. In Fig. 5 we plot the maximum three-body scattering length in units of two-body BB (BI) scattering length $a_{\rm BB}$ ($a_{\rm BI}$) as a function of the square root of the mass ratio $\sqrt{M/m}$ with fixed $g_0/d_0 = 4$. Altering the mass ratio $\sqrt{M/m}$ can change g/d. The relation between $\sqrt{M/m}$ and g/d is shown in Fig. 2 by a red (dark gray) solid line. The numerical result shows that there are some singularities, which occur at green dashed lines, as shown in Fig. 5.

As we can see from Fig. 5, by increasing $\sqrt{M/m}$ from $\sqrt{M/m} = 4$ (the case in Fig. 4), $a_{\rm max,BI,BB}$ increases until it meets infinity at $\sqrt{M/m} = 5.06$, which results in the intersection value of the parameter $a_{\rm BI}\kappa$ of three-body bound state and the atom-dimer continuum going from a certain value to infinity. In this sense, at $\sqrt{M/m} = 5.06$, there are four three-body bound states for arbitrary a_3, among which the one with the smallest κ is induced by three-body interaction. This statement can be verified by comparing with Fig. 2. The system without three-body interaction meets the transition point from three to four three-body bound states at $\sqrt{M/m} = 5.06$ and $|d_0|/|g_0| = 4$. Continuously increasing $\sqrt{M/m}$ until 5.57, there are five three-body bound states when $a_{\rm max,BB,BI}$ increases from 0 (at the exact point $a_{\rm max,BB,BI} = 0$ there are actually four three-body bounded states induced by two-body interaction, which can also be verified by comparing with Fig. 2) to a certain value. Among the five three-body bound states the one with the smallest κ is induced by three-body interaction. At $\sqrt{M/m} = 5.57$, we have $d/g = 1$. Increasing $\sqrt{M/m}$ again, $a_{\rm max,BB,BI}$ begins to decrease. This

turning point is nonsmooth, which is a result of the nonsmooth change of threshold from $\sqrt{M/m} < 5.57$ $(d/g < 1)$ to $\sqrt{M/m} > 5.57$ $(d/g > 1)$. With $\sqrt{M/m} < 5.57$ and $\sqrt{M/m} > 5.57$, the thresholds are $E_{\rm th} = -\hbar^2(g/2)^2/(2\mu_{12,3})$ and $E_{\rm th} = -\hbar^2(d/2)^2/(2\mu_{12,3})$, of which the first-order derivatives are discontinued at $\sqrt{M/m} = 5.57$. The reason $a_{\rm max,BB,BI}$ is a monotonically increasing (decreasing) function of the mass ratio for $\sqrt{M/m} < 5.57$ ($\sqrt{M/m} > 5.57$) is that the number of three-body bound states induced only by two-body interaction is increasing (decreasing) at $\sqrt{M/m} < 5.57$ ($\sqrt{M/m} > 5.57$) (see Fig. 2 for reference). If we keep increasing $\sqrt{M/m}$ to 5.61, $a_{\rm max,BB,BI}$ decreases to 0, which suggests the disappearance of one three-body bound state. At $\sqrt{M/m} = 5.61$, only four three-body bound states remain, which all result from two-body interaction. Again increasing $\sqrt{M/m}$ until 6.1, $a_{\rm max,BB,BI}$ decreases from infinity to zero. In this interval, we have three three-body bound states induced by two-body interaction.

An interesting fact is that the locations of the green dashed lines in Fig. 5 match exactly with the intersection of the red line and the phase boundaries in Fig. 2. This can be understood as when $a_{\rm max,BB,BI} = 0$, the energy of the three-body bound state induced by two-body interaction with the lowest κ approaches the atom-dimer continuum spectrum at $a_3 \to \infty$, where the particles experience no three-body interaction. This is exactly the condition for the transition of the number of two-body interactions inducing three-body bound states to occur without three-body interaction. The explanation above also works for why there is always an additional three-body bound state in the mass-balanced case. The intersection of the dashed line $(M/m = 1)$ and dotted line $(|d|/|g| = 1)$ in Fig. 2 is a transition point when varying the mass ratio along an interval containing $M/m = 1$ with fixed $|d|/|g|$.

VI. SUMMARY

We have studied the bound states of a 1D three-body mass-imbalanced system with two-body attractive interaction. In the absence of three-body interaction, we presented the phase diagram of the number of three-body bound states by solving the STM equations with arbitrary d/g and M/m. We developed some computational techniques and applied them to obtain the complete phase diagram. We demonstrated that the LLH system has at most three three-body bound states. In particular, in the limit of $M/m \to 0$ the LLH system has the Bethe-ansatz solution, which further verifies the validity of our results. Moreover, we found that the presence of the three-body interaction may lead to one more bound state. However, this additional three-body bound state would not always exist, but depends on the mass ratio and the ratio of coupling strength d_0/g_0. The existence of the additional three-body bound state is independent of the three-body interaction at some special parameter points which correspond to the transition points of the number of three-body bound states induced solely by two-body attractive interaction.

The techniques to solve the STM equations may be applied to study mass-imbalanced four-body or N-body systems. Our results may help in understanding how mass-imbalanced particles are bound with two-body attractive interactions and three-body interaction.

ACKNOWLEDGMENTS

The work was supported by NSFC under Grant No. 11974413, the National Key Research and Development Program of China under Grant No. 2016YFA0300600, and the Strategic Priority Research Program of Chinese Academy of Sciences under Grant No. XDB33000000. Y.-C.Y. was supported by the National Science Foundation for Young Scientists of China under Grant No. 11804377.

APPENDIX: LARGE MOMENTUM BEHAVIOR OF SOLUTIONS OF EQS. (7) AND (13)

Equation (7) can be rewritten as

$$f_i(k) = \sum_{j\neq i} \int dk' f_j(k') G_{i,j}(k,k'), \tag{A1}$$

where

$$G_{i,j}(k,k') = \frac{1}{\left(1+\frac{g_i}{2\sqrt{k^2+\kappa^2}}\right)} \times \sum_{j\neq i} \int \frac{dk'}{2\pi} \frac{-g_j|\sin(\theta_i-\theta_j)|}{k'^2+k^2-2kk'\cos(\theta_i-\theta_j)+\kappa^2\sin^2(\theta_i-\theta_j)}. \tag{A2}$$

Expanding $G_{i,j}(k,k')$ at $1/k \to 0$, we obtain

$$G_{i,j}(k,k') = \frac{-g_j|\sin(\theta_i-\theta_j)|}{k^2} + o\left(\frac{1}{k^3}\right). \tag{A3}$$

In addition, $f_i(k)$ at large momentum is

$$f_i(k) = \frac{A_i}{k^2} + o\left(\frac{1}{k^3}\right), \tag{A4}$$

where $A_i = -\sum_{j\neq i} g_j|\sin(\theta_i-\theta_j)| \int dk' f_j(k')$. So $f_i(k) \propto \frac{1}{k^2}$ in the ultraviolet region.

Similarly, Eq. (13) can be rewritten as

$$F_i(k) = -\frac{1}{\left(1+\frac{g_i}{2\sqrt{k^2+\kappa^2}}\right)} \frac{\pi}{\sqrt{k^2+\kappa^2}} + \sum_{j\neq i} \int dk' F_j(k') G_{i,j}(k,k'). \tag{A5}$$

By large momentum expansion,

$$F_i(k) + \frac{\pi}{\sqrt{k^2+\kappa^2}} = \frac{A_i + \frac{\pi g_i}{2}}{k^2} + o\left(\frac{1}{k^3}\right). \tag{A6}$$

Thus, $F_i(k) \approx -\frac{\pi}{\sqrt{k^2+\kappa^2}}$ and $F_i(k) + \frac{\pi}{\sqrt{k^2+\kappa^2}} \propto \frac{1}{k^2}$ in the ultraviolet region.

[1] E. Nielsen, D. Fedorov, A. Jensen, and E. Garrido, The three-body problem with short-range interactions, Phys. Rep. **347**, 373 (2001).

[2] E. Braaten and H.-W. Hammer, Universality in few-body systems with large scattering length, Phys. Rep. **428**, 259 (2006).

[3] C. H. Greene, P. Giannakeas, and J. Pérez-Ríos, Universal few-body physics and cluster formation, Rev. Mod. Phys. **89**, 035006 (2017).

[4] P. Naidon and S. Endo, Efimov physics: A review, Rep. Prog. Phys. **80**, 056001 (2017).

[5] G. V. Skorniakov and K. A. Ter-Martirosian, Three body problem for short range forces. I. Scattering of low energy neutrons by deuterons, Sov. Phys. JETP **4**, 648 (1957).

[6] L. D. Faddeev, Mathematical questions in the quantum theory of scattering for a system of three particles, Tr. Mat. Inst. Steklov. **69**, 3 (1963).

[7] V. Efimov, Energy levels arising from resonant two-body forces in a three-body system, Phys. Lett. B **33**, 563 (1970).

[8] V. Efimov, Weakly-bound states of three resonantly-interacting particles, Yad. Fiz. **12**, 1080 (1970) [Sov. J. Nucl. Phys. **12**, 589 (1971)].

[9] T. Kraemer, M. Mark, P. Waldburger, J. G. Danzl, C. Chin, B. Engeser, A. D. Lange, K. Pilch, A. Jaakkola, H.-C. Nägerl, and R. Grimm, Evidence for Efimov quantum states in an ultracold gas of caesium atoms, Nature (London) **440**, 315 (2006).

[10] E. Braaten and H.-W. Hammer, Efimov physics in cold atoms, Ann. Phys. (NY) **322**, 120 (2007).

[11] F. Ferlaino and R. Grimm, Trend: Forty years of Efimov physics: How a bizarre prediction turned into a hot topic, Physics **3**, 9 (2010).

[12] M. Zaccanti, B. Deissler, C. D'Errico, M. Fattori, M. Jona-Lasinio, S. Müller, G. Roati, M. Inguscio, and G. Modugno, Observation of an Efimov spectrum in an atomic system, Nat. Phys. **5**, 586 (2009).

[13] Y. Nishida, Y. Kato, and C. D. Batista, Efimov effect in quantum magnets, Nat. Phys. **9**, 93 (2013).

[14] M. Kunitski, S. Zeller, J. Voigtsberger, A. Kalinin, L. P. H. Schmidt, M. Schöffler, A. Czasch, W. Schöllkopf, R. E. Grisenti, T. Jahnke, D. Blume, and R. Dörner, Observation of the Efimov state of the helium trimer, Science **348**, 551 (2015).

[15] D. C. Mattis, The few-body problem on a lattice, Rev. Mod. Phys. **58**, 361 (1986).

[16] Z.-Y. Shi, X. Cui, and H. Zhai, Universal Trimers Induced by Spin-Orbit Coupling in Ultracold Fermi Gases, Phys. Rev. Lett. **112**, 013201 (2014).

[17] X. Cui and W. Yi, Universal Borromean Binding in Spin-Orbit-Coupled Ultracold Fermi Gases, Phys. Rev. X **4**, 031026 (2014).

[18] Q. Guan and D. Blume, Three-Boson Spectrum in the Presence of 1D Spin-Orbit Coupling: Efimov's Generalized Radial Scaling Law, Phys. Rev. X **8**, 021057 (2018).

[19] Y. Nishida, S. Moroz, and D. T. Son, Super Efimov Effect of Resonantly Interacting Fermions in Two Dimensions, Phys. Rev. Lett. **110**, 235301 (2013).

[20] S. Moroz, J. P. D'Incao, and D. S. Petrov, Generalized Efimov Effect in One Dimension, Phys. Rev. Lett. **115**, 180406 (2015).

[21] C. Chin, R. Grimm, P. Julienne, and E. Tiesinga, Feshbach resonances in ultracold gases, Rev. Mod. Phys. **82**, 1225 (2010).

[22] G. Guijarro, A. Pricoupenko, G. E. Astrakharchik, J. Boronat, and D. S. Petrov, One-dimensional three-boson problem with two- and three-body interactions, Phys. Rev. A **97**, 061605(R) (2018).

[23] Y. Nishida, Universal bound states of one-dimensional bosons with two- and three-body attractions, Phys. Rev. A **97**, 061603(R) (2018).

[24] C. Mora, R. Egger, and A. O. Gogolin, Three-body problem for ultracold atoms in quasi-one-dimensional traps, Phys. Rev. A **71**, 052705 (2005).

[25] O. I. Kartavtsev, A. V. Malykh, and S. A. Sofianos, Bound states and scattering lengths of three two-component particles with zero-range interactions under one-dimensional confinement, J. Exp. Theor. Phys. **108**, 365 (2009).

[26] N. P. Mehta, Born-Oppenheimer study of two-component few-particle systems under one-dimensional confinement, Phys. Rev. A **89**, 052706 (2014).

[27] N. P. Mehta and C. D. Morehead, Few-boson processes in the presence of an attractive impurity under one-dimensional confinement, Phys. Rev. A **92**, 043616 (2015).

[28] L. Happ, M. Zimmermann, S. I. Betelu, W. P. Schleich, and M. A. Efremov, Universality in a one-dimensional three-body system, Phys. Rev. A **100**, 012709 (2019).

[29] L. Pricoupenko, Three-body pseudopotential for atoms confined in one dimension, Phys. Rev. A **99**, 012711 (2019).

[30] N. Harshman and A. Knapp, Anyons from three-body hard-core interactions in one dimension, Ann. Phys. (NY) **412**, 168003 (2020).

[31] I. E. Mazets, T. Schumm, and J. Schmiedmayer, Breakdown of Integrability in a Quasi-1D Ultracold Bosonic Gas, Phys. Rev. Lett. **100**, 210403 (2008).

[32] S. Tan, M. Pustilnik, and L. I. Glazman, Relaxation of a High-Energy Quasiparticle in a One-Dimensional Bose Gas, Phys. Rev. Lett. **105**, 090404 (2010).

[33] D. S. Petrov, V. Lebedev, and J. T. M. Walraven, Controlling integrability in a quasi-one-dimensional atom-dimer mixture, Phys. Rev. A **85**, 062711 (2012).

[34] T. Kristensen and L. Pricoupenko, One-dimensional ultracold atomic gases: Impact of the effective range on integrability, Phys. Rev. A **93**, 023629 (2016).

[35] A. Lamacraft, Diffractive scattering of three particles in one dimension: A simple result for weak violations of the Yang-Baxter equation, Phys. Rev. A **87**, 012707 (2013).

[36] E. H. Lieb and W. Liniger, Exact analysis of an interacting Bose gas. I. The general solution and the ground state, Phys. Rev. **130**, 1605 (1963).

[37] J. B. McGuire, Study of exactly soluble one-dimensional N-body problems, J. Math. Phys. **5**, 622 (1964).

[38] M. Valiente, Three-body repulsive forces among identical bosons in one dimension, Phys. Rev. A **100**, 013614 (2019).

[39] A. Pricoupenko and D. S. Petrov, Higher-order effective interactions for bosons near a two-body zero crossing, Phys. Rev. A **103**, 033326 (2021).

[40] Y. Sekino and Y. Nishida, Quantum droplet of one-dimensional bosons with a three-body attraction, Phys. Rev. A **97**, 011602(R) (2018).

[41] A. Pricoupenko and D. S. Petrov, Dimer-dimer zero crossing and dilute dimerized liquid in a one-dimensional mixture, Phys. Rev. A **97**, 063616 (2018).

[42] I. Morera, B. Juliá-Díaz, and M. Valiente, Quantum liquids and droplets with low-energy interactions in one dimension, arXiv:2103.16499.

[43] M. Girardeau, Relationship between systems of impenetrable bosons and fermions in one dimension, J. Math. Phys. **1**, 516 (1960).

[44] T. Cheon and T. Shigehara, Fermion-Boson Duality of One-Dimensional Quantum Particles with Generalized Contact Interactions, Phys. Rev. Lett. **82**, 2536 (1999).

[45] M. D. Girardeau and M. Olshanii, Theory of spinor Fermi and Bose gases in tight atom waveguides, Phys. Rev. A **70**, 023608 (2004).

[46] M. Valiente, Bose-Fermi dualities for arbitrary one-dimensional quantum systems in the universal low-energy regime, Phys. Rev. A **102**, 053304 (2020).

[47] Y. Sekino and Y. Nishida, Field-theoretical aspects of one-dimensional Bose and Fermi gases with contact interactions, Phys. Rev. A **103**, 043307 (2021).

[48] M. Valiente, Universal duality transformations in interacting one-dimensional quantum systems, Phys. Rev. A **103**, L021302 (2021).

[49] E. Wille, F. M. Spiegelhalder, G. Kerner, D. Naik, A. Trenkwalder, G. Hendl, F. Schreck, R. Grimm, T. G. Tiecke, J. T. M. Walraven, S. J. J. M. F. Kokkelmans, E. Tiesinga, and P. S. Julienne, Exploring an Ultracold Fermi-Fermi Mixture: Interspecies Feshbach Resonances and Scattering Properties of ^{6}Li and ^{40}K, Phys. Rev. Lett. **100**, 053201 (2008).

[50] T. G. Tiecke, M. R. Goosen, A. Ludewig, S. D. Gensemer, S. Kraft, S. J. J. M. F. Kokkelmans, and J. T. M. Walraven, Broad Feshbach Resonance in ^{6}Li-^{40}K Mixture, Phys. Rev. Lett. **104**, 053202 (2010).

[51] M. Cetina, M. Jag, R. S. Lous, I. Fritsche, J. T. M. Walraven, R. Grimm, J. Levinsen, M. M. Parish, R. Schmidt, M. Knap, and E. Demler, Ultrafast many-body interferometry of impurities coupled to a Fermi sea, Science **354**, 96 (2016).

[52] C. Ravensbergen, V. Corre, E. Soave, M. Kreyer, E. Kirilov, and R. Grimm, Production of a degenerate Fermi-Fermi mixture of dysprosium and potassium atoms, Phys. Rev. A **98**, 063624 (2018).

[53] Z. Hadzibabic, C. A. Stan, K. Dieckmann, S. Gupta, M. W. Zwierlein, A. Grlitz, and W. Ketterle, Two-Species Mixture of Quantum Degenerate Bose and Fermi Gases, Phys. Rev. Lett. **88**, 160401 (2002).

[54] K. Günter, T. Stöferle, H. Moritz, M. Köhl, and T. Esslinger, Bose-Fermi Mixtures in a Three-Dimensional Optical Lattice, Phys. Rev. Lett. **96**, 180402 (2006).

[55] T. Best, S. Will, U. Schneider, L. Hackermüller, D. van Oosten, I. Bloch, and D.-S. Lühmann, Role of Interactions in ^{87}Rb-^{40}K Bose-Fermi Mixtures in a 3D Optical Lattice, Phys. Rev. Lett. **102**, 030408 (2009).

[56] C.-H. Wu, I. Santiago, J. W. Park, P. Ahmadi, and M. W. Zwierlein, Strongly interacting isotopic Bose-Fermi mixture immersed in a Fermi sea, Phys. Rev. A **84**, 011601(R) (2011).

[57] S.-K. Tung, K. Jiménez-García, J. Johansen, C. V. Parker, and C. Chin, Geometric Scaling of Efimov States in a ^{6}Li-^{133}Cs Mixture, Phys. Rev. Lett. **113**, 240402 (2014).

[58] R. S. Lous, I. Fritsche, M. Jag, F. Lehmann, E. Kirilov, B. Huang, and R. Grimm, Probing the Interface of a Phase-Separated State in a Repulsive Bose-Fermi Mixture, Phys. Rev. Lett. **120**, 243403 (2018).

[59] L. A. Zundel, J. M. Wilson, N. Malvania, L. Xia, J.-F. Riou, and D. S. Weiss, Energy-Dependent Three-Body Loss in 1D Bose Gases, Phys. Rev. Lett. **122**, 013402 (2019).

[60] M. Born and R. Oppenheimer, Zur quantentheorie der molekeln, Ann. Phys. (Leipzig) **389**, 457 (1927).

[61] P. Cheiney, C. R. Cabrera, J. Sanz, B. Naylor, L. Tanzi, and L. Tarruell, Bright Soliton to Quantum Droplet Transition in a Mixture of Bose-Einstein Condensates, Phys. Rev. Lett. **120**, 135301 (2018).

[62] S. Weinberg, Systematic solution of multiparticle scattering problems, Phys. Rev. **133**, B232 (1964).

[63] C. Thorn, Quark confinement in the infinite-momentum frame, Phys. Rev. D **19**, 639 (1979).

[64] H. E. Camblong and C. R. Ordonez, Renormalized path integral for the two-dimensional δ-function interaction, Phys. Rev. A **65**, 052123 (2002).

[65] S. Coleman and E. Weinberg, Radiative corrections as the origin of spontaneous symmetry breaking, Phys. Rev. D **7**, 1888 (1973).

[66] L. D. Faddeev, Notes on divergences and dimensional transmutation in Yang—Mills theory, Theor. Math. Phys. **148**, 986 (2006).

[67] H. E. Camblong, L. N. Epele, H. Fanchiotti, and C. A. G. Canal, Dimensional transmutation and dimensional regularization in quantum mechanics, Ann. Phys. (NY) **287**, 14 (2001).